Front. Phys., 2014, 9(2): 246–254
DOI 10.1007/s11467-013-0368-y

RESEARCH ARTICLE

Two-dimensional MRT LB model for compressible and incompressible flows

Feng Chen[1,*], **Ai-Guo Xu**[2,†], **Guang-Cai Zhang**[2], **Yong-Long Wang**[3]

[1] *School of Aeronautics, Shan Dong Jiaotong University, Jinan 250357, China*

[2] *National Key Laboratory of Computational Physics, Institute of Applied Physics and Computational Mathematics, P. O. Box 8009-26, Beijing 100088, China*

[3] *Institute of Condensed Matter Physics, School of Science, Linyi University, Linyi 276005, China*

*Corresponding authors. E-mail: * shanshiwycf@163.com, † Xu_Aiguo@iapcm.ac.cn*

Received May 21, 2013; accepted July 16, 2013

In the paper we extend the Multiple-Relaxation-Time (MRT) Lattice Boltzmann (LB) model proposed in [*Europhys. Lett.*, 2010, 90: 54003] so that it is suitable also for incompressible flows. To decrease the artificial oscillations, the convection term is discretized by the flux limiter scheme with splitting technique. A new model is validated by some well-known benchmark tests, including Riemann problem and Couette flow, and satisfying agreements are obtained between the simulation results and analytical ones. In order to show the merit of LB model over traditional methods, the non-equilibrium characteristics of system are solved. The simulation results are consistent with the physical analysis.

Keywords lattice Boltzmann method, multiple-relaxation-time, flux limiter technique, Prandtl numbers effect, non-equilibrium characteristic

PACS numbers 47.11.-j, 51.10.+y, 05.20.Dd

1 Introduction

In recent years, the Lattice Boltzmann (LB) method has emerged as an attractive computational approach for complex physical system [1–7]. The lattice Bhatnagar–Gross–Krook (BGK) model, based on a single-relaxation-time approximation, is the simplest and the most popular form. However, this simplicity also leads to some deficiencies, such as the numerical stability problem, and fixed Prandtl number. To overcome these deficiencies of BGK model, the Multiple-Relaxation-Time (MRT) lattice Boltzmann method [8–10] has been developed, and successfully used in simulating various fluid flow problems [11–20]. Most of the existing MRT models work only for isothermal system. To simulate system with temperature field, many attempts have been made [21–23].

Besides the models mentioned above, we proposed an MRT Finite Difference lattice Boltzmann model for compressible flows with arbitrary specific heat ratio and Prandtl number in previous work [24]. In the model, the kinetic moment space and the equilibria of nonconserved moments are constructed according to the seven-moment relations associated with the local equilibrium distribution function. Numerical experiments showed that compressible flows with strong shocks can be well simulated by this model.

In the paper we extend the MRT LB model so that it is suitable also for incompressible flows. In order to efficiently decrease the unphysical oscillations, the flux limiter scheme [25–28] with splitting technique is incorporated into the new model. When the system deviates more from equilibrium, the LB simulation can give more physical information [29–31], such as the non-equilibrium characteristics of system. Here, in the new MRT LB model, the non-equilibrium characteristics of system are solved through a dynamic procedure where a shock wave propagates from a heavy medium to a light one.

The rest of the paper is organized as follows. Section 2 presents the extended MRT LB model. Section 3 describes the finite difference schemes. Section 4 is for the validation and verification of the new LB model. Non-equilibrium characteristics are shown and analyzed in Section 5. Section 6 makes the conclusion for the present paper.

© Higher Education Press and Springer-Verlag Berlin Heidelberg 2014

2 Model description

According to the main strategy of MRT LB method, the MRT LB equation can be described as:

$$\frac{\partial f_i}{\partial t} + v_{i\alpha}\frac{\partial f_i}{\partial x_\alpha} = -\boldsymbol{M}_{il}^{-1}\hat{\boldsymbol{S}}_{lk}(\hat{f}_k - \hat{f}_k^{eq}) \tag{1}$$

where f_i and $\hat{f}_i$ are the particle distribution function in the velocity space and the kinetic moment space respectively, $\boldsymbol{v}_i$ is the discrete particle velocity, $i = 1, \cdots, N$, N is the number of discrete velocities, the subscript α indicates x or y. The matrix $\hat{\boldsymbol{S}} = \boldsymbol{MSM}^{-1} = diag(s_1, s_2, \cdots, s_N)$ is the diagonal relaxation matrix. $\boldsymbol{M}$ is the transformation matrix between the velocity space and the kinetic moment space. $\hat{f}_i = m_{ij}f_j$, m_{ij} is an element of the transformation matrix. $\hat{f}_i^{eq}$ is the equilibrium value of distribution function $\hat{f}_i$ in the kinetic moment space.

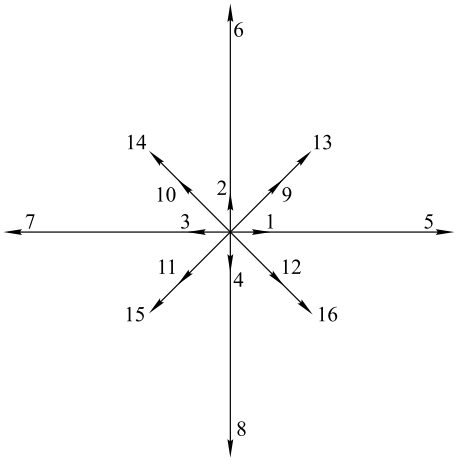

Fig. 1 Schematics of $\boldsymbol{v}_i$ for the discrete velocity model.

In the previous work, we constructed a two-dimensional MRT LB model based on the model by Kataoka and Tsutahara [32] (see Fig. 1):

$$(v_{i1}, v_{i2}) = \begin{cases} \textbf{cyc}: (\pm 1, 0), & \text{for } 1 \leqslant i \leqslant 4 \\ \textbf{cyc}: (\pm 6, 0), & \text{for } 5 \leqslant i \leqslant 8 \\ \sqrt{2}(\pm 1, \pm 1), & \text{for } 9 \leqslant i \leqslant 12 \\ \dfrac{3}{\sqrt{2}}(\pm 1, \pm 1), & \text{for } 13 \leqslant i \leqslant 16 \end{cases}$$

where **cyc** indicates the cyclic permutation. Transformation matrix $\boldsymbol{M}$ and the equilibrium distribution function $\hat{f}_i^{eq}$ in the moment space are chosen according to the seven-moment relations (see Appendix for details). At the continuous limit, the above formulation recovers the following Navier–Stokes (NS) equations:

$$\frac{\partial \rho}{\partial t} + \frac{\partial(\rho u_x)}{\partial x} + \frac{\partial(\rho u_y)}{\partial y} = 0 \tag{2a}$$

$$\begin{aligned} &\frac{\partial(\rho u_x)}{\partial t} + \frac{\partial}{\partial x}(\rho u_x^2) + \frac{\partial}{\partial y}(\rho u_x u_y) \\ &= -\frac{\partial P}{\partial x} + \frac{\partial}{\partial y}[\frac{\rho RT}{s_7}(\frac{\partial u_y}{\partial x} + \frac{\partial u_x}{\partial y})] \\ &\quad + \frac{\partial}{\partial x}[\frac{\rho RT}{s_5}(1 - \frac{2}{b})(\frac{\partial u_x}{\partial x} + \frac{\partial u_y}{\partial y}) \\ &\quad + \frac{\rho RT}{s_6}(\frac{\partial u_x}{\partial x} - \frac{\partial u_y}{\partial y})] \end{aligned} \tag{2b}$$

$$\begin{aligned} &\frac{\partial(\rho u_y)}{\partial t} + \frac{\partial}{\partial x}(\rho u_x u_y) + \frac{\partial}{\partial y}(\rho u_y^2) \\ &= -\frac{\partial P}{\partial y} + \frac{\partial}{\partial x}[\frac{\rho RT}{s_7}(\frac{\partial u_y}{\partial x} + \frac{\partial u_x}{\partial y})] \\ &\quad + \frac{\partial}{\partial y}[\frac{\rho RT}{s_5}(1 - \frac{2}{b})(\frac{\partial u_x}{\partial x} + \frac{\partial u_y}{\partial y}) \\ &\quad - \frac{\rho RT}{s_6}(\frac{\partial u_x}{\partial x} - \frac{\partial u_y}{\partial y})] \end{aligned} \tag{2c}$$

$$\begin{aligned} &\frac{\partial e}{\partial t} + \frac{\partial}{\partial x}[(e + 2P)u_x] + \frac{\partial}{\partial y}[(e + 2P)u_y] \\ &= 2\frac{\partial}{\partial x}\Big\{\frac{\rho RT}{s_8}[(\frac{b}{2} + 1)R\frac{\partial T}{\partial x} + (2\frac{\partial u_x}{\partial x} - \frac{2}{b}\frac{\partial u_x}{\partial x} \\ &\quad - \frac{2}{b}\frac{\partial u_y}{\partial y})u_x + (\frac{\partial u_y}{\partial x} + \frac{\partial u_x}{\partial y})u_y]\Big\} \\ &\quad + 2\frac{\partial}{\partial y}\Big\{\frac{\rho RT}{s_9}[(\frac{b}{2} + 1)R\frac{\partial T}{\partial y} + (\frac{\partial u_y}{\partial x} + \frac{\partial u_x}{\partial y})u_x \\ &\quad + (2\frac{\partial u_y}{\partial y} - \frac{2}{b}\frac{\partial u_x}{\partial x} - \frac{2}{b}\frac{\partial u_y}{\partial y})u_y]\Big\} \end{aligned} \tag{2d}$$

where $P = \rho RT$, $e = b\rho RT + \rho u_\alpha^2$ is twice of the total energy, and b is a constant related to the specific-heat-ratio $\gamma = (b + 2)/b$.

In order to maintain the isotropy constraint of viscous stress tensor and heat conductivity, some of the relaxation parameters should be equal to one another, namely $s_5 = s_6 = s_7$, $s_8 = s_9$. The above NS equations reduce to

$$\frac{\partial \rho}{\partial t} + \frac{\partial(\rho u_\alpha)}{\partial x_\alpha} = 0 \tag{3a}$$

$$\begin{aligned} &\frac{\partial(\rho u_\alpha)}{\partial t} + \frac{\partial(\rho u_\alpha u_\beta)}{\partial x_\beta} = -\frac{\partial P}{\partial x_\alpha} + \frac{\partial}{\partial x_\beta}[\mu(\frac{\partial u_\alpha}{\partial x_\beta} \\ &\quad + \frac{\partial u_\beta}{\partial x_\alpha} - \frac{2}{3}\frac{\partial u_\chi}{\partial x_\chi}\delta_{\alpha\beta}) + \mu_B\frac{\partial u_\chi}{\partial x_\chi}\delta_{\alpha\beta}] \end{aligned} \tag{3b}$$

$$\begin{aligned} &\frac{\partial e}{\partial t} + \frac{\partial}{\partial x_\alpha}[(e + 2P)u_\alpha] = 2\frac{\partial}{\partial x_\beta}[(\frac{b}{2} + 1)\lambda' R\frac{\partial T}{\partial x_\beta} \\ &\quad + \lambda'(\frac{\partial u_\alpha}{\partial x_\beta} + \frac{\partial u_\beta}{\partial x_\alpha} - \frac{2}{b}\frac{\partial u_\chi}{\partial x_\chi}\delta_{\alpha\beta})u_\alpha] \end{aligned} \tag{3c}$$

where the viscosity $\mu = \rho RT/s_5$, the bulk viscosity

$\mu_B = (2/3 - 2/b)\rho RT/s_5$, $\lambda' = \rho RT/s_8$, $(\alpha, \beta, \chi = x, y)$.

However, the viscous coefficient in the energy equation (3c) is not consistent with that in the momentum equation (3b). By modifying the collision operators of the moments related to energy flux:

$$\begin{aligned}\hat{\boldsymbol{S}}_{88}(\hat{f}_8 - \hat{f}_8^{eq}) \Rightarrow\ & \hat{\boldsymbol{S}}_{88}(\hat{f}_8 - \hat{f}_8^{eq}) + (s_8/s_5 - 1)\rho T u_x \\ & \times(4\frac{\partial u_x}{\partial x} - \frac{4}{b}\frac{\partial u_x}{\partial x} - \frac{4}{b}\frac{\partial u_y}{\partial y}) \\ & +(s_8/s_5 - 1)\rho T u_y(2\frac{\partial u_y}{\partial x} + 2\frac{\partial u_x}{\partial y}) \qquad (4a)\end{aligned}$$

$$\begin{aligned}\hat{\boldsymbol{S}}_{99}(\hat{f}_9 - \hat{f}_9^{eq}) \Rightarrow\ & \hat{\boldsymbol{S}}_{99}(\hat{f}_9 - \hat{f}_9^{eq}) + (s_9/s_5 - 1)\rho T u_x \\ & \times(2\frac{\partial u_y}{\partial x} + 2\frac{\partial u_x}{\partial y}) \\ & +(s_9/s_5 - 1)\rho T u_y(4\frac{\partial u_y}{\partial y} - \frac{4}{b}\frac{\partial u_x}{\partial x} - \frac{4}{b}\frac{\partial u_y}{\partial y}) \qquad (4b)\end{aligned}$$

we get the following energy equation:

$$\begin{aligned}&\frac{\partial e}{\partial t} + \frac{\partial}{\partial x_\alpha}[(e + 2P)u_\alpha] \\ &= 2\frac{\partial}{\partial x_\beta}[\lambda\frac{\partial T}{\partial x_\beta} + \mu(\frac{\partial u_\alpha}{\partial x_\beta} + \frac{\partial u_\beta}{\partial x_\alpha} - \frac{2}{b}\frac{\partial u_\chi}{\partial x_\chi}\delta_{\alpha\beta})u_\alpha] \qquad (5)\end{aligned}$$

where the thermal conductivity $\lambda = (\frac{b}{2} + 1)R\lambda'$.

3 Finite difference scheme

In the original LB model [24], the time evolution is based on the usual first-order forward Euler scheme, while space discretization is performed through a Lax-Wendroff scheme. In this work, the flux limiter scheme with splitting technique corresponding to the MRT model is adopted. The proposed flux limiter scheme can efficiently decrease the unphysical oscillations around the interfaces.

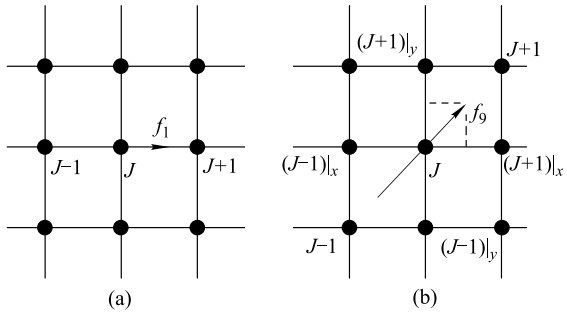

Fig. 2 Characteristic lines and corresponding projections in the x and y directions. **(a)** $f_1(\boldsymbol{x}, t)$; **(b)** $f_9(\boldsymbol{x}, t)$.

Figure 2 shows the characteristic lines in the flux limiter scheme and corresponding projections in x and y directions. $(J-1)\big|_x$ and $(J-1)\big|_y$ are corresponding projections of node $J-1$ in the x and y directions. Let $f_{i,J}^n$ be the value of distribution function at time t in the node J along the direction i, we rewrite the evolution of f_i in node J at time step $t + dt$ as follows:

$$\begin{aligned}f_{i,J}^{n+1} = f_{i,J}^n &- \frac{\mathrm{d}t}{A_i \mathrm{d}x}[F_{i,J+1/2}^n\big|_x - F_{i,J-1/2}^n\big|_x] \\ &- \frac{\mathrm{d}t}{A_i \mathrm{d}y}[F_{i,J+1/2}^n\big|_y - F_{i,J-1/2}^n\big|_y] \\ &- \mathrm{d}t\mathbf{M}_{il}^{-1}\hat{\mathbf{S}}_{lk}(\hat{f}_{k,J}^n - \hat{f}_{k,J}^{n,eq}) \qquad (6)\end{aligned}$$

where

$$A_i = \begin{cases} 1, & \text{for } 1 \leqslant i \leqslant 4 \\ 1/6, & \text{for } 5 \leqslant i \leqslant 8 \\ 1/\sqrt{2}, & \text{for } 9 \leqslant i \leqslant 12 \\ \sqrt{2}/3, & \text{for } 13 \leqslant i \leqslant 16 \end{cases} \qquad (7)$$

$F_{i,J+1/2}^n\big|_x$ $(F_{i,J-1/2}^n\big|_x)$ and $F_{i,J+1/2}^n\big|_y$ $(F_{i,J-1/2}^n\big|_y)$ are x and y components of the outgoing (incoming) flux in node J along the direction i,

$$\begin{aligned}F_{i,J+1/2}^n\big|_x &= f_i^n(ix, iy) + \frac{1}{2}(1 - \frac{\mathrm{d}t}{A_i \mathrm{d}x}) \\ &\times[f_i^n(ix + A_i v_{ix}, iy) - f_i^n(ix, iy)]\psi_x(ix, iy) \qquad (8a) \\ F_{i,J-1/2}^n\big|_x &= f_i^n(ix - A_i v_{ix}, iy) + \frac{1}{2}(1 - \frac{\mathrm{d}t}{A_i \mathrm{d}x}) \\ &\times[f_i^n(ix, iy) - f_i^n(ix - A_i v_{ix}, iy)]\psi_x(ix - A_i v_{ix}, iy) \qquad (8b) \\ F_{i,J+1/2}^n\big|_y &= f_i^n(ix, iy) + \frac{1}{2}(1 - \frac{\mathrm{d}t}{A_i \mathrm{d}y}) \\ &\times[f_i^n(ix, iy + A_i v_{iy}) - f_i^n(ix, iy)]\psi_y(ix, iy) \qquad (8c) \\ F_{i,J-1/2}^n\big|_y &= f_i^n(ix, iy - A_i v_{iy}) + \frac{1}{2}(1 - \frac{\mathrm{d}t}{A_i \mathrm{d}y}) \\ &\times[f_i^n(ix, iy) - f_i^n(ix, iy - A_i v_{iy})]\psi_y(ix, iy - A_i v_{iy}) \qquad (8d)\end{aligned}$$

The flux limiter is expressed as

$$\psi_\alpha(ix, iy) = \begin{cases} 0, & \theta_i^n(ix, iy)\big|_\alpha \leqslant 0 \\ 2\theta_i^n(ix, iy)\big|_\alpha, & 0 \leqslant \theta_i^n(ix, iy)\big|_\alpha \leqslant \frac{1}{3} \\ (1 + \theta_i^n(ix, iy)\big|_\alpha)/2, & \frac{1}{3} \leqslant \theta_i^n(ix, iy)\big|_\alpha \leqslant 3 \\ 2, & 3 \leqslant \theta_i^n(ix, iy)\big|_\alpha \end{cases} \qquad (9)$$

where the smoothness functions are

$$\theta_i^n(ix, iy)\big|_x = \frac{f_i^n(ix, iy) - f_i^n(ix - A_i v_{ix}, iy)}{f_i^n(ix + A_i v_{ix}, iy) - f_i^n(ix, iy)} \qquad (10a)$$

$$\theta_i^n(ix, iy)\big|_y = \frac{f_i^n(ix, iy) - f_i^n(ix, iy - A_i v_{iy})}{f_i^n(ix, iy + A_i v_{iy}) - f_i^n(ix, iy)} \qquad (10b)$$

The Lax–Wendroff scheme is recovered for the flux limiter $\psi_x = \psi_y = 1$, and the first order upwind scheme is recovered when $\psi_x = \psi_y = 0$.

4 Validation and verification

4.1 Performance on discontinuity

In order to check the performance of flux limiter scheme on discontinuity, we construct the following problem

$$\begin{cases} (\rho, u_1, u_2, T) = (1.5, 0.666667, 0.0, 1.55556), \\ \qquad x \leqslant L/2 \\ (\rho, u_1, u_2, T) = (1.0, 0.0, 0.0, 1.0), \\ \qquad L/2 < x < L \end{cases} \tag{11}$$

L is the length of computational domain. In the x direction, $f_i = \boldsymbol{M}_{ij}^{-1} \hat{f}_j^{eq}$ is set, where the macroscopic quantities adopt the initial values. In the y direction, the periodic boundary condition is adopted. The physical quantities on the two sides satisfy the Hugoniot relations. Figure 3 shows the simulation results of the density, pressure, $x-$ component of velocity, and temperature at time $t = 0.06$ with use of different space discretization schemes. The parameters are $\gamma = 2$, $\mathrm{d}x = \mathrm{d}y = 0.001$, $\mathrm{d}t = 10^{-5}$, $s_5 = s_6 = s_7 = 5 \times 10^4$, and other collision parameters are 10^5. The simulations with Lax–Wendroff scheme have strong unphysical oscillations in the shocked region. The second order upwind scheme results in unphysical "overshoot" phenomena at the shock front. The simulation results with the flux limiter scheme are much more accurate, and this scheme has the ability to decrease the unphysical oscillations at the discontinuity.

4.2 Lax shock tube problem

The initial condition of the problem is

$$\begin{cases} (\rho, u_1, u_2, T) = (0.445, 0.698, 0.0, 7.928), \\ \qquad x \leqslant L/2 \\ (\rho, u_1, u_2, T) = (0.5, 0.0, 0.0, 1.142), \\ \qquad L/2 < x < L \end{cases} \tag{12}$$

The profiles of density, pressure, $x-$ component of velocity, and temperature at $t = 0.45$ are shown in Fig. 4, where the exact solutions are presented with solid lines for comparison. The parameters are $\gamma = 1.4$, $\mathrm{d}x = \mathrm{d}y = 0.003$, $\mathrm{d}t = 10^{-5}$, $s_5 = s_6 = s_7 = 2 \times 10^3$, $s_8 = s_9 = 10^3$, and other collision parameters are 10^5. Obviously, the simulation results agree well with the exact solutions.

The above simulations show that compressible flows, especially those with discontinuity and shock waves, can be well simulated by the present model.

4.3 Couette flow

Here we conduct a series of numerical simulations of Couette flow. In the simulation, the left wall is fixed and the right wall moves at speed $u_x = 0$, $u_y = 0.1$. The initial

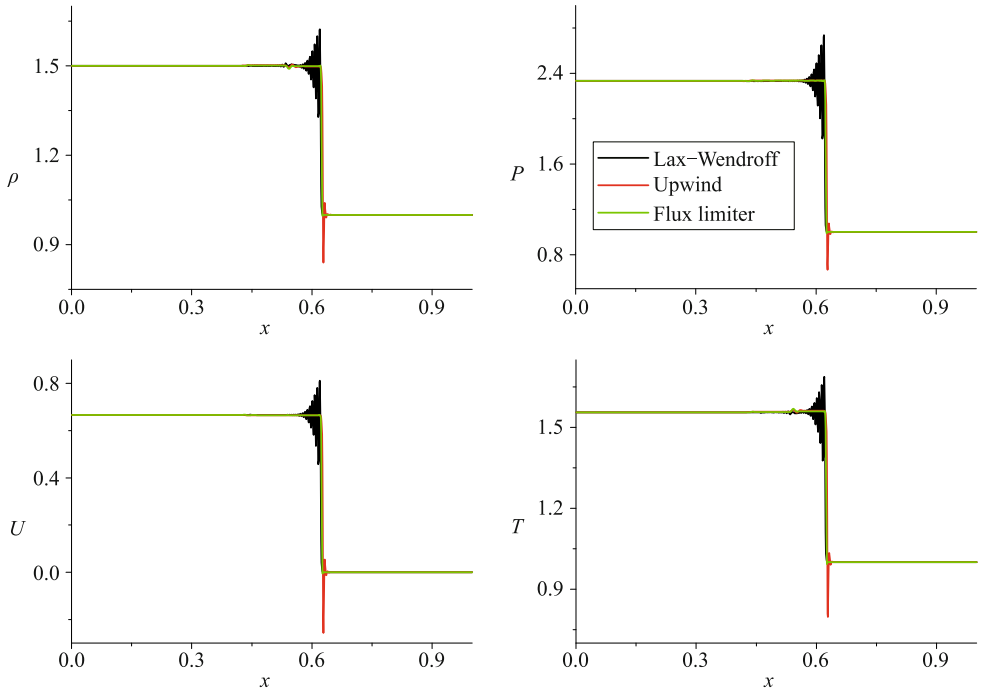

Fig. 3 Simulation results with various difference schemes at $t = 0.06$.

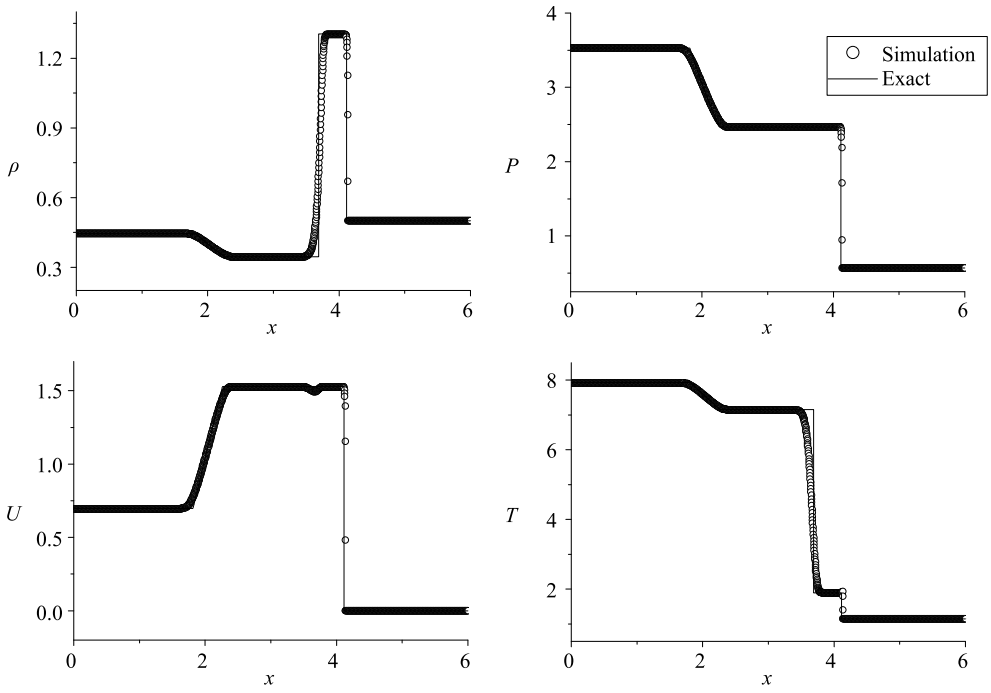

Fig. 4 LB simulation results and exact solutions for Lax shock tube at $t = 0.45$.

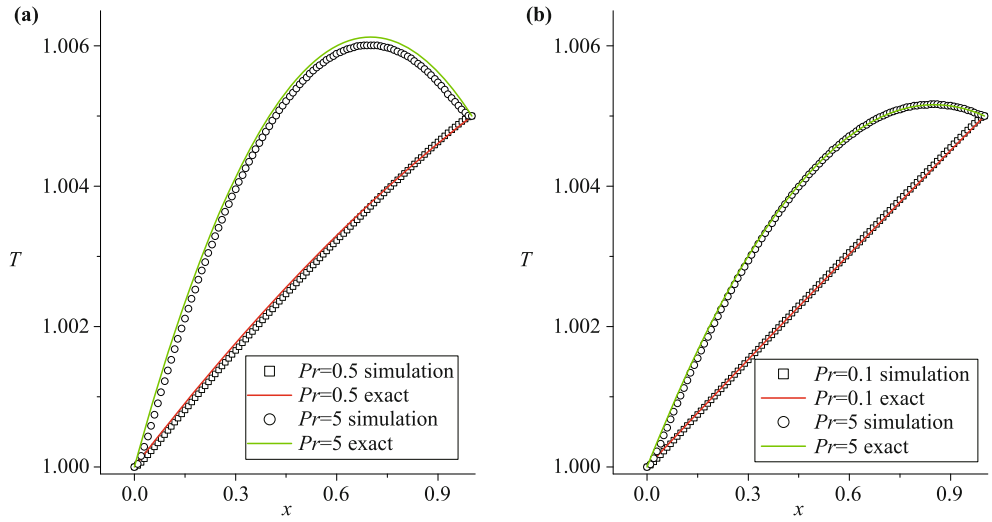

Fig. 5 Temperature profiles of Couette flow. **(a)** $\gamma = 2$, $Pr = 0.5$ corresponds to $s_5 = 10^3, s_8 = 5 \times 10^2$, $Pr = 5$ corresponds to $s_5 = 2 \times 10^2, s_8 = 10^3$, and **(b)** $\gamma = 1.4$, $Pr = 0.1$ corresponds to $s_5 = 10^3, s_8 = 10^2$, $Pr = 5$ corresponds to $s_5 = 2 \times 10^2, s_8 = 10^3$ (other collision parameters are 10^3).

state of the fluid is $\rho = 1$, $T = 1$, $u_x = 0$, $u_y = 0$. The simulation results are compared with the analytical solution:

$$T = T_1 + (T_2 - T_1)\frac{x}{H} + \frac{\mu}{2\lambda}u_y^2\frac{x}{H}(1 - \frac{x}{H}) \qquad (13)$$

where T_1 and T_2 are temperatures of the left and right walls ($T_1 = 1$, $T_2 = 1.005$), H is the width of the channel. Periodic boundary conditions are applied to the bottom and top boundaries, and the left and right walls adopt the nonequilibrium extrapolation method. Figure 5 shows the comparison of LB results with analytical solutions for thermal Couette Flows. (a) corresponds to $\gamma = 2$, and (b) corresponds to $\gamma = 1.4$. It is clearly shown that the simulation results of the new model are in agreement with the analytical solutions, and the Prandtl number effects are successfully captured. The new model is suitable for incompressible flows.

5 Non-equilibrium characteristic

To show the merit of LB method over traditional ones,

in this section we study the non-equilibrium characteristics using the new model. Among the moment relations required by each LB model, the equilibrium distribution function f_i^{eq} can be replaced by the distribution function f_i only for the first three (density, momentum and energy). If we replace f_i^{eq} by f_i in the left hand of other moment relations, the value of the left side will have a difference from that of the right side. This difference represents the deviation of the system from its thermodynamic equilibrium [29–31]. In this MRT LB model, the kinetic moment space and the corresponding equilibria of nonconserved moments are constructed according to the seven-moment relations. So, the deviation from equilibrium in this model can be defined as $\Delta_i = \hat{f}_i - \hat{f}_i^{eq} = \boldsymbol{M}_{ij}(f_j - f_j^{eq})$. Δ_i contains the information of macroscopic flow velocity u_α. Furthermore, we replace $v_{i\alpha}$ by $v_{i\alpha} - u_\alpha$ in the transformation matrix $\boldsymbol{M}$, named $\boldsymbol{M}^*$ (see Appendix for details). $\Delta_i^* = \boldsymbol{M}_{ij}^*(f_j - f_j^{eq})$ is only the manifestation of molecular thermalmotion and does not contain the information of macroscopic flow.

Now, we study the following dynamic procedure. An incident shock wave with Mach number 1.414 travels from a heavy medium and hits a light one, where the two different fluids are separated by an unperturbed interface. The initial macroscopic quantity is as follows:

$$\begin{cases} (\rho, u_1, u_2, p)_s = (1.5, 0.666667, 0, 2.33334) \\ (\rho, u_1, u_2, p)_h = (1, 0, 0, 1) \\ (\rho, u_1, u_2, p)_l = (0.5, 0, 0, 1) \end{cases}$$

where the subscripts s, h, l indicate the shock wave region, the heavy medium region, and the light medium region, respectively. In our simulations, the computational domain is $[0, 1.2] \times [0, 0.01]$, and is divided into 1200×10 mesh-cells. The initial position of the shock wave is $x = 0.24$, the unperturbed interface lies at the position $x = 0.4$. The inflow boundary is applied at the left side, the outflow boundary is applied at the right side, and periodic boundary conditions are applied at the top and bottom boundaries. $\gamma = 2$ in the whole domain. The density, pressure, $x-$ component of velocity and temperature profiles and Δ_i^* $(i = 5, 6, 7, 10, 11)$ on the center line $y = 0.005$ at time $t = 0.3$ are shown in Fig. 6. The parameters are $\mathrm{d}t = 10^{-5}$, $s_5 = s_6 = s_7 = 5 \times 10^4$, and other collision parameters are 10^5.

In the figures, the system shows three different interfaces, rarefaction wave, material interface, and shock wave. The physical quantity changes significantly at the three interfaces, and the vertical lines indicate the

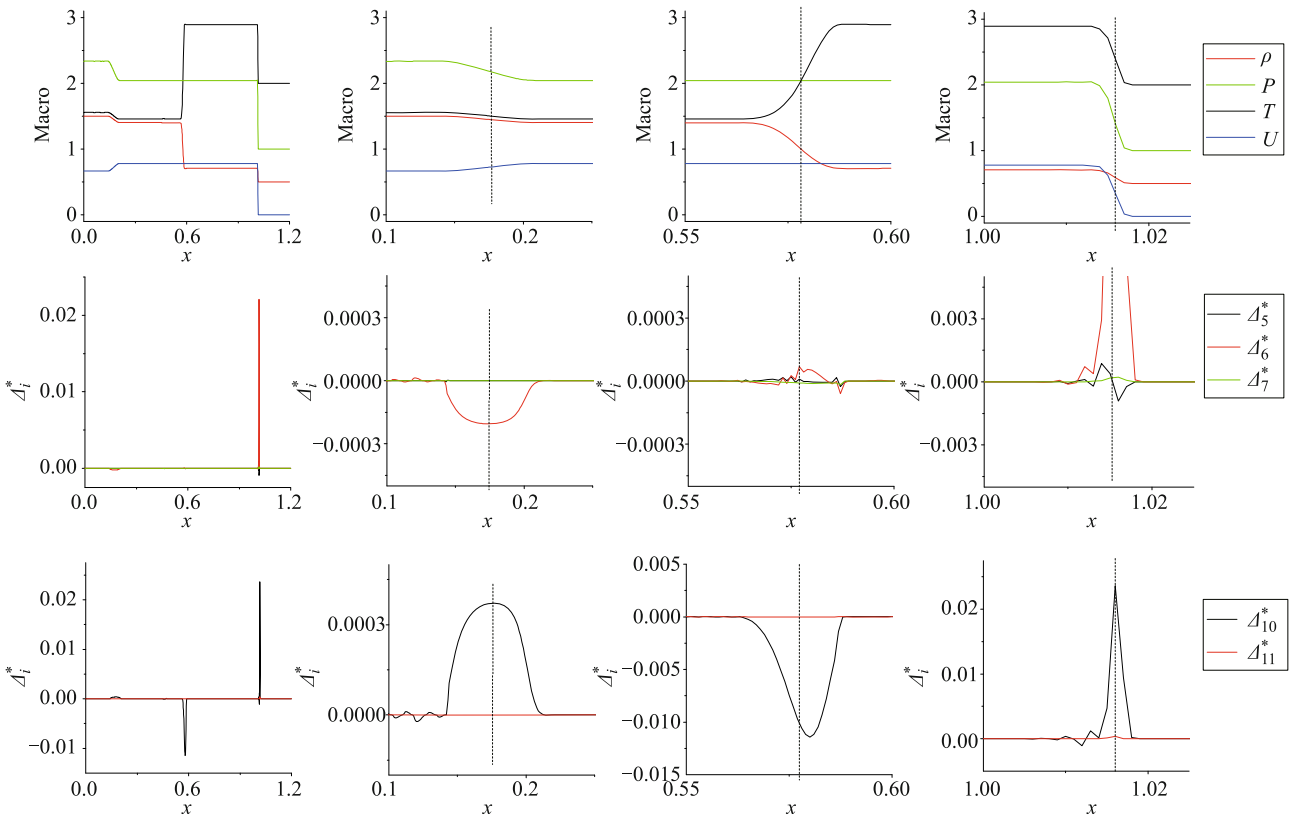

Fig. 6 LB numerical results and non-equilibrium characteristics at $t = 0.3$.

positions of interfaces. The system starts to deviate from equilibrium once the physical quantity starts to change. When the physical quantity arrives at its steady-state required by the Hugoniot relations, the system goes back to its equilibrium state. The peak values of deviations Δ_i^* at the shock wave interface are larger than the others. This is because the shock dynamic procedure is faster than the other two processes, and the system has less time to relax to its thermodynamic equilibrium.

At the interfaces, Δ_5^*, Δ_7^* and Δ_{11}^* have small amplitudes. Δ_5^* contains two parts, x and y components of internal translational kinetic energy. This indicates that the two parts deviate from equilibrium in opposite directions with the same amplitude. Δ_6^* shows an opposite deviation for the rarefaction wave interface and the shock interface. The physical reason is as below. The temperature gradient first initiates variance of the internal kinetic energy in the direction of temperature gradient. (Here, the temperature shows gradient in the x direction.) Then, part of the internal kinetic energy variance is transferred to other degrees of freedoms via collisions of molecules. The internal kinetic energy in the temperature gradient direction further varies, and so on. The shock wave increases the density, pressure and temperature, while the rarefaction wave decreases those quantities. So, Δ_6^* shows a negative deviation for the rarefaction wave interface while showing a positive deviation for the shock interface. The values of Δ_{10}^* at the material interface and shock wave interface have the same order, and are much larger than that at rarefaction wave. This is because the sizes of temperature variation near the material interface and shock wave differ little, and are larger than that near the rarefaction wave. When the temperature gradient vanishes, the system attains its thermodynamic equilibrium.

6 Conclusions

In the paper an MRT LB model for compressible flows is extended so that it is suitable also for incompressible flows. In order to efficiently decrease the unphysical oscillations, space discretization adopts the flux limiter scheme with splitting technique. It is validated and verified via same well-known benchmark tests, including Riemann problem and Couette flow, and satisfying agreements are obtained between the new model results and analytical ones. In order to show the merit of LB model over traditional methods, we studied the behaviors of system deviating from its equilibrium through a dynamic procedure where shock wave propagates from a heavy material to a light one. The simulation results are consistent with the physical analysis.

Acknowledgements The authors would like to sincerely thank S. Succi and C. Lin for many instructive discussions. We acknowledge support of National Natural Science Foundation of China (under Grant Nos. 11075021 and 11047020). A. G. Xu and G. C. Zhang acknowledge support of the Science Foundation of CAEP (Grant Nos. 2012B0101014 and 2011A0201002) and the Foundation of State Key Laboratory of Explosion Science and Technology (Grant No. KFJJ14-1M).

Appendix A: Transformation matrix and equilibria of the nonconserved moments

In the model by Kataoka and Tsutahara, the local equilibrium distribution function f_i^{eq} satisfies the following relations:

$$\rho = \sum f_i^{eq} \tag{A1a}$$

$$\rho u_\alpha = \sum f_i^{eq} v_{i\alpha} \tag{A1b}$$

$$\rho(bRT + u_\alpha^2) = \sum f_i^{eq}(v_{i\alpha}^2 + \eta_i^2) \tag{A1c}$$

$$P\delta_{\alpha\beta} + \rho u_\alpha u_\beta = \sum f_i^{eq} v_{i\alpha} v_{i\beta} \tag{A1d}$$

$$\rho[(b+2)RT + u_\beta^2]u_\alpha = \sum f_i^{eq}(v_{i\beta}^2 + \eta_i^2)v_{i\alpha} \tag{A1e}$$

$$\rho[RT(u_\alpha\delta_{\beta\chi} + u_\beta\delta_{\alpha\chi} + u_\chi\delta_{\alpha\beta}) + u_\alpha u_\beta u_\chi] = \sum f_i^{eq} v_{i\alpha} v_{i\beta} v_{i\chi} \tag{A1f}$$

$$\rho\{(b+2)R^2T^2\delta_{\alpha\beta} + [(b+4)u_\alpha u_\beta + u_\chi^2\delta_{\alpha\beta}]RT + u_\chi^2 u_\alpha u_\beta\} = \sum f_i^{eq}(v_{i\chi}^2 + \eta_i^2)v_{i\alpha}v_{i\beta} \tag{A1g}$$

where a parameter η_i is introduced, in order to describe the $(b-2)$ extra-degrees of freedom corresponding to molecular rotation and/or vibration, where $\eta_i = 5/2$ for $i = 1, \cdots, 4$, and $\eta_i = 0$ for $i = 5, \cdots, 16$.

The transformation matrix $\boldsymbol{M}$ in the MRT model is composed as below: $\boldsymbol{M} = (m_1, m_2, \cdots, m_{16})^{\mathrm{T}}$,

$$m_{1i} = 1 \tag{A2a}$$

$$m_{2i} = v_{ix} \tag{A2b}$$

$$m_{3i} = v_{iy} \tag{A2c}$$

$$m_{4i} = v_{ix}^2 + v_{iy}^2 + \eta_i^2 \tag{A2d}$$

$$m_{5i} = v_{ix}^2 + v_{iy}^2 \tag{A2e}$$

$$m_{6i} = v_{ix}^2 - v_{iy}^2 \tag{A2f}$$

$$m_{7i} = v_{ix}v_{iy} \tag{A2g}$$

$$m_{8i} = v_{ix}(v_{ix}^2 + v_{iy}^2 + \eta_i^2) \tag{A2h}$$

$$m_{9i} = v_{iy}(v_{ix}^2 + v_{iy}^2 + \eta_i^2) \tag{A2i}$$

$$m_{10i} = v_{ix}(v_{ix}^2 + v_{iy}^2) \tag{A2j}$$

$$m_{11i} = v_{iy}(v_{ix}^2 + v_{iy}^2) \tag{A2k}$$

$$m_{12i} = v_{ix}(v_{ix}^2 - v_{iy}^2) \tag{A2l}$$
$$m_{13i} = v_{iy}(v_{ix}^2 - v_{iy}^2) \tag{A2m}$$
$$m_{14i} = (v_{ix}^2 + v_{iy}^2)(v_{ix}^2 + v_{iy}^2 + \eta_i^2) \tag{A2n}$$
$$m_{15i} = v_{ix}v_{iy}(v_{ix}^2 + v_{iy}^2 + \eta_i^2) \tag{A2o}$$
$$m_{16i} = (v_{ix}^2 - v_{iy}^2)(v_{ix}^2 + v_{iy}^2 + \eta_i^2) \tag{A2p}$$

where $i = 1, \cdots, 16$.

Replacing $v_{i\alpha}$ by $v_{i\alpha} - u_\alpha$ in the transformation matrix $\boldsymbol{M}$, matrix $\boldsymbol{M}^*$ is expressed as follows: $\boldsymbol{M}^* = (m_1^*, m_2^*, \cdots, m_{16}^*)^{\mathrm{T}}$,

$$m_{1i}^* = 1 \tag{A3a}$$
$$m_{2i}^* = v_{ix} - u_x \tag{A3b}$$
$$m_{3i}^* = v_{iy} - u_y \tag{A3c}$$
$$m_{4i}^* = (v_{ix} - u_x)^2 + (v_{iy} - u_y)^2 + \eta_i^2 \tag{A3d}$$
$$m_{5i}^* = (v_{ix} - u_x)^2 + (v_{iy} - u_y)^2 \tag{A3e}$$
$$m_{6i}^* = (v_{ix} - u_x)^2 - (v_{iy} - u_y)^2 \tag{A3f}$$
$$m_{7i}^* = (v_{ix} - u_x)(v_{iy} - u_y) \tag{A3g}$$
$$m_{8i}^* = (v_{ix} - u_x)[(v_{ix} - u_x)^2 + (v_{iy} - u_y)^2 + \eta_i^2] \tag{A3h}$$
$$m_{9i}^* = (v_{iy} - u_y)[(v_{ix} - u_x)^2 + (v_{iy} - u_y)^2 + \eta_i^2] \tag{A3i}$$
$$m_{10i}^* = (v_{ix} - u_x)[(v_{ix} - u_x)^2 + (v_{iy} - u_y)^2] \tag{A3j}$$
$$m_{11i}^* = (v_{iy} - u_y)[(v_{ix} - u_x)^2 + (v_{iy} - u_y)^2]) \tag{A3k}$$
$$m_{12i}^* = (v_{ix} - u_x)[(v_{ix} - u_x)^2 - (v_{iy} - u_y)^2] \tag{A3l}$$
$$m_{13i}^* = (v_{iy} - u_y)[(v_{ix} - u_x)^2 - (v_{iy} - u_y)^2] \tag{A3m}$$
$$m_{14i}^* = [(v_{ix} - u_x)^2 + (v_{iy} - u_y)^2][(v_{ix} - u_x)^2 + (v_{iy} - u_y)^2 + \eta_i^2] \tag{A3n}$$
$$m_{15i}^* = (v_{ix} - u_x)(v_{iy} - u_y)[(v_{ix} - u_x)^2 + (v_{iy} - u_y)^2 + \eta_i^2] \tag{A3o}$$
$$m_{16i}^* = [(v_{ix} - u_x)^2 - (v_{iy} - u_y)^2][(v_{ix} - u_x)^2 + (v_{iy} - u_y)^2 + \eta_i^2] \tag{A3p}$$

where $i = 1, \cdots, 16$.

The equilibria of nonconserved moments are as follows:

$$\hat{f}_5^{eq} = 2P + (j_x^2 + j_y^2)/\rho \tag{A4a}$$
$$\hat{f}_6^{eq} = (j_x^2 - j_y^2)/\rho \tag{A4b}$$
$$\hat{f}_7^{eq} = j_x j_y/\rho \tag{A4c}$$
$$\hat{f}_8^{eq} = (e + 2P)j_x/\rho \tag{A4d}$$
$$\hat{f}_9^{eq} = (e + 2P)j_y/\rho \tag{A4e}$$
$$\hat{f}_{10}^{eq} = (4P + j_x^2/\rho + j_y^2/\rho)j_x/\rho \tag{A4f}$$
$$\hat{f}_{11}^{eq} = (4P + j_x^2/\rho + j_y^2/\rho)j_y/\rho \tag{A4g}$$
$$\hat{f}_{12}^{eq} = (2P + j_x^2/\rho - j_y^2/\rho)j_x/\rho \tag{A4h}$$
$$\hat{f}_{13}^{eq} = (-2P + j_x^2/\rho - j_y^2/\rho)j_y/\rho \tag{A4i}$$
$$\hat{f}_{14}^{eq} = 2(b+2)\rho R^2T^2 + (6+b)RT(j_x^2 + j_y^2)/\rho + (j_x^2 + j_y^2)^2/\rho^3 \tag{A4j}$$
$$\hat{f}_{15}^{eq} = [(b+4)P + (j_x^2 + j_y^2)/\rho]j_x j_y/\rho^2 \tag{A4k}$$
$$\hat{f}_{16}^{eq} = [(b+4)P + (j_x^2 + j_y^2)/\rho](j_x^2 - j_y^2)/\rho^2 \tag{A4l}$$

References

1. S. Succi, The Lattice Boltzmann Equation for Fluid Dynamics and Beyond, Oxford: Oxford University Press, 2001
2. R. Benzi, S. Succi, and M. Vergassola, The lattice Boltzmann equation: Theory and applications, *Phys. Rep.*, 1992, 222(3): 145
3. A. G. Xu, G. Gonnella, and A. Lamura, Phase-separating binary fluids under oscillatory shear, *Phys. Rev. E*, 2003, 67(5): 056105
4. A. G. Xu, G. Gonnella, and A. Lamura, Morphologies and flow patterns in quenching of lamellar systems with shear, *Phys. Rev. E*, 2006, 74(1): 011505
5. A. G. Xu, G. Gonnella, and A. Lamura, Phase separation of incompressible binary fluids with lattice Boltzmann methods, *Physica A*, 2004, 331(1–2): 10
6. A. G. Xu, G. Gonnella, and A. Lamura, Numerical study of the ordering properties of lamellar phase, *Physica A*, 2004, 344(3–4): 750
7. A. G. Xu, G. Gonnella, and A. Lamura, Simulations of complex fluids by mixed lattice Boltzmann-finite difference methods, *Physica A*, 2006, 362(1): 42
8. F. J. Higuera, S. Succi, and R. Benzi, Lattice gas dynamics with enhanced collisions, *Europhys. Lett.*, 1989, 9: 345
9. F. J. Higuera and J. Jimenez, Boltzmann approach to lattice gas simulations, *Europhys. Lett.*, 1989, 9: 662
10. D. d'Humieres, Generalized lattice-Boltzmann equations, in: Rarefied Gas Dynamics: Theory and Simulations, edited by B. D. Shizgal and D. P Weaver, Progress in Astronautics and Aeronautics, Vol. 159, Washington: AIAA Press, DC, 1992: 450-458
11. P. Lallemand and L. S. Luo, Theory of the lattice Boltzmann method: Dispersion, dissipation, isotropy, Galilean invariance, and stability, *Phys. Rev. E*, 2000, 61(6): 6546
12. D. d'Humières, M. Bouzidi, and P. Lallemand, Thirteen-velocity three-dimensional lattice Boltzmann model, *Phys. Rev. E*, 2001, 63(6): 066702
13. M. E. McCracken and J. Abraham, Multiple-relaxation-time lattice-Boltzmann model for multiphase flow, *Phys. Rev. E*, 2005, 71(3): 036701
14. K. N. Premnath and J. Abraham, Three-dimensional multi-relaxation time (MRT) lattice-Boltzmann models for multiphase flow, *J. Comput. Phys.*, 2007, 224(2): 539
15. H. D. Yu, L. S. Luo, and S. S. Girimaji, LES of turbulent square jet flow using an MRT lattice Boltzmann model, *Comput. Fluids*, 2006, 35(8–9): 957

16. P. Asinari, Asymptotic analysis of multiple-relaxation-time lattice Boltzmann schemes for mixture modeling, *Comput. Math. Appl.*, 2008, 55(7): 1392
17. I. Rasin, S. Succi, and W. Miller, A multi-relaxation lattice kinetic method for passive scalar diffusion, *J. Comput. Phys.*, 2006, 206(2): 453
18. H. Yoshida and M. Nagaoka, Multiple-relaxation-time lattice Boltzmann model for the convection and anisotropic diffusion equation, *J. Comput. Phys.*, 2010, 229(20): 7774
19. Z. H. Chai and T. S. Zhao, Effect of the forcing term in the multiple-relaxation-time lattice Boltzmann equation on the shear stress or the strain rate tensor, *Phys. Rev. E*, 2012, 86(1): 016705
20. J. J. Huang, H. B. Huang, C. Shu, Y. T. Chew, and S. L. Wang, Hybrid multiple-relaxation-time lattice-Boltzmann finite-difference method for axisymmetric multiphase flows, *J. Phys. A: Math. Theor.*, 2013, 46(5): 055501
21. P. Lallemand and L. S. Luo, Theory of the lattice Boltzmann method: Acoustic and thermal properties in two and three dimensions, *Phys. Rev. E*, 2003, 68(3): 036706
22. L. Zheng, B. C. Shi, and Z. L. Guo, Multiple-relaxation-time model for the correct thermohydrodynamic equations, *Phys. Rev. E*, 2008, 78(2): 026705
23. A. Mezrhab, M. A. Moussaouia, M. Jami, H. Naji, and M. Bouzidi, Double MRT thermal lattice Boltzmann method for simulating convective flows, *Phys. Lett. A*, 2010, 374(34): 3499
24. F. Chen, A. G. Xu, G. C. Zhang, Y. J. Li, and S. Succi, Multiple-relaxation-time lattice Boltzmann approach to compressible flows with flexible specific-heat ratio and Prandtl number, *Europhys. Lett.*, 2010, 90(5): 54003
25. A. Cristea and V. Sofonea, Two component lattice Boltzmann model with flux limiter techniques, *Proceedings of the Romanian Academy, Series A*, 2003, 4: 59
26. A. Cristea and V. Sofonea, Two component lattice Boltzmann model with flux limiters, *Central Eur. J. Phys.*, 2004, 2: 382
27. V. Sofonea, A. Lamura, G. Gonnella, and A. Cristea, Finite-difference lattice Boltzmann model with flux limiters for liquid-vapor systems, *Phys. Rev. E*, 2004, 70(4): 046702
28. F. Chen, A. G. Xu, G. C. Zhang, and Y. J. Li, Flux limiter lattice Boltzmann for compressible flows, *Commun. Theor. Phys.*, 2011, 56(2): 333
29. A. G. Xu, G. C. Zhang, Y. B. Gan, F. Chen, and X. Yu, Lattice Boltzmann modeling and simulation of compressible flows, *Front. Phys.*, 2012, 7(5): 582
30. B. Yan, A. G. Xu, G. C. Zhang, Y. J. Ying, and H. Li, Lattice Boltzmann model for combustion and detonation, *Front. Phys.*, 2013, 8(1): 94
31. C. Lin, A. G. Xu, G. Zhang, Y. Li, and S. Succi, Polar coordinate lattice Boltzmann modeling of compressible flows, arXiv: 1302.7104v1, 2013
32. T. Kataoka and M. Tsutahara, Lattice Boltzmann model for the compressible Navier–Stokes equations with flexible specific-heat ratio, *Phys. Rev. E*, 2004, 69(3): 035701 (R)